Influence of processing severity during equal-channel angular pressing on the microstructure of an Al-Zn-Mg-Cu alloy

C.M. Cepeda-Jiménez[a], J.M. García-Infanta[a], E.F. Rauch[b], J.J. Blandin[b], O.A. Ruano[a], F. Carreño[a]

[a]*Department of Physical Metallurgy, CENIM, CSIC, Av. Gregorio del Amo 8, 28040 Madrid, Spain*

[b]*Laboratoire GPM2, Institut National Polytechnique de Grenoble (INPG), BP 46, 38402 Saint Martin d'Heres, Cedex, France*

Abstract

A commercial Al–Zn–Mg-Cu alloy, Al 7075, was overaged at 280 ºC during 5 h, and processed by equal-channel angular pressing (ECAP) using route B_C. Different temperatures and number of passes, which determine the processing severity, were considered. The processing severity has been estimated by the maximum stress (σ_{Proc}) recorded during each ECAP pass. The higher is the number of passes or lower is the processing temperature, i.e. the higher is the processing severity, the finer is the (sub)grain size obtained. A minimum ultrafine (sub)grain size of approximately 150 nm after 3 passes at 80 ºC or 8 passes at 130 ºC was obtained. The microhardness exhibited an instant increase from 76 HV for the overaged initial state to 115 HV after only the first pass. The coarsened precipitates in the overaged alloy lead to larger structural refinement than in pure aluminum.

Keywords: Aluminum alloys; Equal-channel angular pressing (ECAP); Microstructure; Transmission electron microscopy (TEM)

*Corresponding author. Tel.: +34 91 5538900 ext.217; fax: +34 91 5347425.
E-mail address: cm.cepeda@cenim.csic.es (C.M. Cepeda-Jiménez)

1. Introduction

The need for low weight airframes has led to the development of very high-strength alloys used as plates, sheets and extrusions. The highest room temperature strengths attained in wrought aluminum alloy products correspond to the aluminum–zinc–magnesium–copper alloys [1,2]. Among the 7xxx series alloys, the Al 7075 has been

widely used in commercial applications because it exhibits high strength and can be heat-treated to a variety of microstructures [3].

However, additional homogenization and refinement of such microstructures by severe plastic deformation (SPD) processing is beneficial to improve the mechanical properties at ambient temperature, and to obtain a rapid superplastic forming at relatively low temperatures, providing that the developed ultrafine grains are stable at such temperatures [4].

Equal channel angular pressing (ECAP) is a very interesting method for modifying microstructure, producing ultra fine grained (UFG) materials [5-11]. In an idealized description of ECAP, deformation takes place by simple shear confined to a narrow zone at the plane of intersection of die channels, as illustrated in Fig. 1, without any change in cross-sectional area upon passage through the intersection of the die channels. This process is, therefore, amenable to repetition [12]. The repetitive pressings also provide an opportunity for initiating new slip systems by rotating the sample about the longitudinal axis between consecutive passes [13]. It has been shown experimentally that, when using an ECAP die with an angle of 90° between the two parts of the channel, optimum processing is achieved using route B_C, which is referred to a rotation through 90° in the same direction between consecutive passes. This route leads most rapidly both to an array of reasonably equiaxed grains, and to a high fraction of grain boundaries having high angles of misorientation [14]. The process of ECAP was proven [15-21] to be an effective tool for both increasing the strength and toughness. In addition, if the ultrafine grain sizes are retained to elevated temperature where diffusion becomes quite rapid, there is a possibility of achieving a superplastic forming capability even at high strain rates [22].

A careful inspection of the literature shows that the strategy followed in the majority of SPD processed Al alloys to stabilize the microstructure at high temperature is to add small amounts of elements such as Sc and Zr [23-25]. A fine dispersion of Al_3Sc and/or Al_3Zr formed during casting acts inhibiting grain growth at high temperatures. Consequently, high strain rate superplasticity (HSRS) has been observed at high temperatures. Since Sc and Zr are expensive, such additions to the composition of widely employed alloys such as the Al 7075, would raise the production costs.

On the other hand, to date, much of the research on ECAP has concentrated on relatively soft materials such as pure fcc metals or solid solution alloys. By contrast, there have been only a limited number of reports on the pressing of more complex alloys, such as Al-Zn-Mg-(Cu) alloys, where aging treatments and precipitation kinetics become important features of the processing method [23-32]. In practice, these alloys

are often difficult to process by ECAP at room temperature because of their very limited formability.

Although there are some reports of the successful ECAP processing of 7xxx series aluminum alloys at room temperature after different thermal treatments [26-28,30], in general, severe plastic deformation leads to an overaging of the samples through the formation of relatively coarse and stable particles. These coarsened particles give an overall reduction in strength. On the other hand, if the 7075 alloy is processed in supersaturated state after solution treatment, the precipitate morphologies are also severely influenced by the pressing operation [32].

Therefore, in the present study the ECAP processing was conducted in the overaged condition, to facilitate the passing through the ECAP die and that large accumulative strains can be introduced. Additionally, it has been reported [33,34] that the presence of overaged second-phase particles favors the structural stability at high temperatures after severe deformation processing, being of considerable importance for retaining high strength and superplastic characteristics. Finally, the strength of the as-received Al 7075 alloy may be essentially restored by conducting an appropriate ageing treatment after the superplastic forming of the final product.

On the other hand, the resulting grain size, L, after thermomechanical processing is usually related to the applied working strain rate and temperature through the Zener-Hollomon parameter, Z, $Z=\dot{\varepsilon}\exp(Q/RT)$. This concept applies to the steady state of the stress-strain curves [35].

The predictions of the resulting grain size using Z are often reported [36-38], and a typical relation between the grain size, L, and Z is the following:

$$\ln L = A - B \ln Z \qquad (1)$$

This equation predicts a fine grain size for high values of Z, i.e., at high strain rates and low temperatures. This equation assumes the subgrain size to be dependent on the stress, σ, (or the strain rate) applied during the test, such that $L \alpha 1/\sigma$.

On the other hand, the Z parameter is usually employed for a given initial microstructure in the material before processing. However, for the ECAP processing different initial microstructures are obtained after consecutive passes, and this cannot be taken properly into account by using the Z parameter.

Up to the present, the severity of a processing has been associated with high strains and fine grain sizes [39-41]. However, strain is not the only factor affecting the microstructure. There are other factors, like the deformation path introduced in the material by the SPD techniques, such as accumulative roll-bonding (ARB), high-pressure torsion (HPT) or ECAP, which frequently involve several deformation cycles and various final stresses applied to the sample during the last cycle. Different

microstructures have been reported to be obtained as a function of the amount of deformation in each pass, for example in ARB [42]), of the applied pressure during HPT [43]) or the channel angle in the ECAP processing [44]). However, no information on the stresses applied to the sample is reported and this is important since the grain size is a function of the stress [45]. It is our contention that the stress applied on the sample during the processing is a better parameter than the strain to describe the processing severity and the final microstructure. Accordingly, to describe correctly the SPD processing and predict the microstructure, the shear torque and the compression stress applied to the sample during the HPT processing, or the electric power consumed during the last cycle of ARB should be determined, since both parameters are directly related to the stress applied on the sample.

In this respect and more easily, the maximum stress given by the testing machine where the ECAP is placed during the ECAP processing is a good estimator of the stress applied on the sample during the processing (σ_{Proc}), and opens new possibilities to predict the microstructure from direct stress data. In the present work, this stress has been termed "processing severity". This is similar to the case of torsion testing, where it is accepted that the torque or its associated stress is related to the subgrain size (L) by the applied stress (σ) such that $L \alpha K/\sigma$, where K is a constant [45].

It is worth noting that the stress state during the ECAP processing is complex. The contribution of various components of the stress, i.e. hydrostatic pressure, friction with the die walls and the flow stress of the sample or resistance of the sample to pass through the channel, are included in the recorded stress during the ECAP processing. Furthermore, these stress components are coupled, being difficult to separate them as independent contributions, and vary simultaneously as a function of the ECAP parameters, such as temperature, number of passes and ECAP path.

However, it is our contention that the processing stress determines the final microstructure and that an inverse relationship, as reported previously [45], exists between the registered stress and the final microstructure, which will allow the prediction of the microstructure under other processing conditions. Accordingly, the changes observed in the processing stress, as a function of ECAP parameters such as T and number of passes that will be varied in this work, will be analyzed in relation with microstructural changes taking place on the sample.

Therefore, the present investigation was initiated to develop an UFG microstructure in a commercial Al 7075 alloy without expensive alloying elements in the composition, and to evaluate the effect of performing ECAP at different processing temperatures (T_p) and number of passes (N_p) on the microstructural evolution. Microstructure evolution has been followed by documenting grain size, shape and distribution of boundary

misorientations. Changes in Vickers microhardness at room temperature observed after severe plastic deformation are examined in terms of the microstructure evolution.

2. Experimental procedure

The as-received aluminum alloy used in the present study was a rolled Al 7075-T651 plate of 12 mm in thickness. The composition in weight percentage of the alloy is included in Table 1.

Al 7075-T651 samples were subjected to an overaging heat treatment at 280 ºC during 5 h prior to the ECAP processing to obtain an stable microstructure and to minimize dynamic processes, such as nucleation and precipitate coarsening during ECAP processing. The nomenclature for the as-started material is Al 7075-O (Table 2).

ECAP billets with dimensions 70 mm × 10 mm × 10 mm were machined along the rolling direction of the as-received plate. ECAP processing was performed using a sharp-cornered 90º ECAP die (zero die-relief angle at the outer corner of the die channel intersection), at a pressing speed of 5 mm/min. Fig. 1 shows the reference axes used in this work, where *z* is the flow plane (FP) normal, *y* the top plane (TP) normal and *x* is the cross-section plane (CP) normal. The shear sense on the shear plane is indicated at the die channel intersection. Samples were ECAP processed by route B_C, i.e. rotated 90° in the same sense between consecutive passes (Fig. 1). This route was selected because it is the optimum processing procedure for attaining superplasticity [46].

Additionally, Table 2 includes the different processing conditions and the nomenclature considered in the present study. The influence of the number of passes and processing temperature has been considered. Each sample was initially pressed once at room temperature (N_p=1), and then pressed repetitively through totals of 3, 5 and 8 passes at 130 ºC, equivalent to imposed strains of ~3, 5 and 8 respectively. The first pass was performed at room temperature to impose high severity to the Al 7075-O alloy and to obtain fine grain size. However, more passes at room temperature without sample cracking were not possible, and a higher processing temperature was considered to facilitate dislocation recovery and the attainment of larger accumulative strains. In addition, samples were ECAP processed through 3 passes at different temperatures, 80, 130 and 180 ºC, to evaluate the influence of processing temperature (T_p). More than 3 passes at 80 ºC were not possible to achieve because visible cracks appeared on the sample surface. On the other hand, no more than 3 passes were carried out at 180 ºC, since considerable grain coarsening was observed. The processing temperature control was carried out by the insertion of two thermocouples in locations close to the die corner.

Fig. 2 shows the load-displacement (F-d) curve for the first pass at room temperature obtained by a universal testing machine coupled to the ECAP equipment. F_{max} is a representative value of the force needed to push the sample through the channel. This value divided by the section of the sample, 1 cm^2, is an estimator of the stress applied on the sample during processing (σ_{Proc}), i.e. the "processing severity".

Optical microscopy and electron backscattered diffraction (EBSD) were employed to characterize the as-started microstructure. The microstructure of processed samples was analyzed by transmission electron microscopy (TEM) using a JEOL JEM 2000 FX II equipment operating at 200 kV. ECAPed samples were always examined at the middle of the ECAP flow plane in order to avoid die wall effects. Samples were ground mechanically to a thickness of ~300 μm, punched into small disks with diameters of 3 mm, and further ground to a thickness of ~100 μm. These small disks were then polished to perforation using a twin-jet electropolishing facility with a solution of 30% nitric acid in methanol at -15 ºC and 15 V. Selected area electron diffraction (SAED) patterns were taken from an area of ~2 μm^2.

EDX analysis to identify the concentration of the precipitates within the as-started Al 7075-O alloy was performed by an electron probe microanalyzer (Oxford Inca) operating at 15 kV, coupled to a scanning electron microscope (SEM) JEOL JSM 6500F equipment with field emission gun.

Grain size was measured for all the processed conditions, from TEM images using the mean linear intercept method, without discriminating between high- and low-angle boundaries, using the Sigma Scan Pro software. More than 300 grains for each processing condition were analyzed. Grain size data fell into log-normal distributions, so the geometric mean value was chosen as a measure of the size.

The microtexture of the ECAPed samples was examined with an automated crystallographic orientation mapping (ACOM) tool attached to a JEOL 3010 TEM operating at 300 kV and equipped with a LaB_6 filament. This technique consists of analyzing spot diffraction patterns [47] rather than Kikuchi lines, which are considered in the EBSD (electron backscattered diffraction) technique that is quite common on modern scanning electron microscopes. For studies involving large strains, the spot patterns are preferred, because they are known to be less sensitive to the internal stresses resulting from severe plastic deformation [48].

The diffraction spot patterns are collected with a digital camera while the thin foil is scanned by the electron beam. Indexing and orientation determination are performed in a single step by comparing an experimental pattern to diffraction pattern templates that were pre-calculated in certain angular steps for all possible orientations of the given crystal structure. The best match gives the correct orientation of the crystal. The

technique therefore does not require the determination of individual spot positions. All spots in the pattern are matched simultaneously, and this creates high confidence and robustness against artifacts [47].

A beam size of 15 nm was used. The diffraction patterns are collected at a rate of 30 frames per second through the frame grabber and the area of interest was typically of 300 x 300 pixels. The step size was 15 nm. The ACOM technique allows to characterize deformed microstructures with (sub)grain size smaller than 100 nm and misorientation $\geq$1º. The use of ACOM allows imaging of the microstructure based on orientation measurements, as well as the presentation of microtexture and grain-boundary data [49]. Color-coded grain-orientation maps were produced by assigning data points to the same grain if neighboring lattice orientations differed by less than 1º. Thus, a low-angle grain boundary (LAB) was defined by a misorientation between adjacent grains of $1º<\theta<15º$, and a high-angle grain boundary (HAB) was defined by $\theta>15º$. HAB and LAB are shown as black and white lines, respectively, on the maps. However, the fraction of high-angle boundaries (f_{HAB}) was calculated from misorientation data higher than 2º. Discrete pole figures were employed to examine the microtexture corresponding to the region investigated.

Vickers microhardness was measured on the flow plane (or z plane) of ECAPed samples using a Matsuzawa Seiki MHT-1 microhardness tester. Loads of 0.5 kg for 15 s, both for the un-processed samples and severely deformed materials, were considered.

3. Results

Fig. 3 shows the processing stress (σ_{Proc}) as a function of N_p for different processing conditions. The first pass was conducted at room temperature and the subsequent passes were performed at three different temperatures. Different trends are observed after the first pass: the stress increases at the lower temperature and decreases for the two higher temperatures. On the other hand, after the second pass the stress, σ_{Proc}, increases with N_p and decreases with T_p, and a saturation value is apparently reached after 6-8 passes at 130 ºC. In addition, it is worth noting that σ_{Proc} values corresponding to the last ECAP pass after the processing paths 3p-80 ºC and 8p-130 ºC are very similar, 790 and 840 MPa respectively. This behavior cannot be understood considering only deformation as a variable. However, the concept of processing severity would allow a good description of the process, and the prediction of the final microstructure as discussed later.

The microstructure of the as-started Al 7075-O is illustrated in Fig. 4 as an isometric optical image. This isometric image has been assembled from optical micrographs obtained on each of three orthogonal planes in each billet. The as-started

Al 7075-O alloy after the overaging treatment shows large grains that are elongated and flattened parallel to the rolling direction. The average grain length in the rolling direction (RD) was about 350 μm.

The microtexture of the as-started Al 7075-O alloy in the LT orientation (longitudinal-transversal) obtained by the electron backscatter diffraction (EBSD) technique attached to a SEM is presented in Fig. 5. The orientation map has been color coded according to the inverse pole figure (IPF) shown in the inset, and the colors represent the crystallographic orientations parallel to the normal direction (ND) of the as-received plate. The orientation map shows elongated grains as a consequence of the rolling processing. The average grain thickness measured from the relative misorientation profile along vertical lines traced in the map is ~15 μm. Although the orientation map was acquired on the LT plane, individual orientations were rotated 90º around RD, to obtain the pole figure corresponding to the longitudinal section or ND plane. The pole figures show a β-fiber texture, characteristic of most rolled face-centered cubic metals [50], even after the overaging treatment.

Characterization at higher magnification by TEM (Fig. 6) reveals two types of precipitates in the as-started Al 7075-O alloy. The EDX peaks from these precipitates are also included in the figure. Peaks appearing in both EDX patterns either were from the aluminum matrix or from precipitates formed during the overaging process. According to the EDX patterns and previous research about characterization of the Al 7075 alloy [51,52], precipitates observed by TEM containing Al, Mg, Zn and Cu correspond to $Mg(Zn_2,AlCu)$. These precipitates are the result of coarsening of η' and η phases during the overaging treatment [51]. On the other hand, particles containing Cr correspond to $Al_{18}Mg_3Cr_2$ precipitates, with significant substitutional presence of Cu, Zn and Ti [52]. The overaging treatment led to the transformation of all these particles to coarser quasi-spheroidized morphologies as illustrated in Fig. 6.

Fig. 7 shows TEM micrographs corresponding to the flow plane of ECAP processed Al 7075-O samples. The black arrows indicate the location of some of the mentioned precipitates. Additionally, corresponding selected-area electron diffraction (SAED) patterns also have been included in Fig. 7.

After one pass (Fig. 7a), it is apparent that the microstructure consists of bands of elongated (sub)grains that are approximately aligned in the shear direction. Since a high density of dislocations in the grains is retained, the grain boundaries are wavy and ill-defined. Observations of this kind demonstrate that the grain boundaries introduced by intense plastic straining are in a high-energy non-equilibrium configuration [53]. The corresponding SAED pattern (inset in Fig. 7a) consists of discrete spots indicating that

the analyzed area presents practically the same crystallographic orientation, and that the (sub)grains are of relatively low misorientation.

Fig. 7b-d show the microstructure of the Al 7075-O alloy after 3, 5 and 8 ECAP passes, respectively, at 130 ºC. The shortest length (L_Y) of the (sub)grain microstructure, which is perpendicular to the elongation direction, was analyzed by mean linear-intercept measurements from these micrographs to quantify the grain refinement. Average values of L_Y as a function of N_p are included in Table 3. It can be observed that the (sub)grain size decreases with N_p from L_Y>400 nm for one pass to L_Y ~ 163 nm for the sample processed by eight passes at 130 ºC. A nearly equiaxed (sub)grain structure after eight ECAP passes (Fig 7d) has replaced the bandlike substructure formed in the initial pressing operation, although a tendency for the (sub)grains to align in the shear direction of the final pressing pass can be observed. The most important change observed with increasing N_p, was the decrease of both the width and the length of the (sub)grains, rapidly for the initial strains (one pass) and more slowly at higher severity levels (Fig. 7 and Table 3). Additionally, there was generally a lower density of intragranular dislocations with an increase in the number of ECAP passes (N_p) (Fig. 7d).

On the other hand, the increase in N_p produces numerous spots in the SAED pattern arranged along circles, especially for 8 ECAP passes, due to different crystallographic orientations, indicating that many boundaries have high misorientation angle.

In addition, inspection of the TEM micrographs in Fig. 7 reveals a large number of fine bright particles distributed through the grains. These coarse spherical precipitates remain apparently unaffected by ECAP processing, with sizes similar to the as-started material (Fig. 6), ranged from ~100 to ~200 nm.

Fig. 8 shows crystallographic orientation maps obtained by the automated electron diffraction pattern indexing tool attached to the TEM (ACOM-TEM). Fig. 8a corresponds to Al 7075-O samples subjected to 3 ECAP passes at 130 ºC, and Fig.8b to 8 passes at 130 ºC. The pole figures {001}, {011}, {111} corresponding to both ECAPed samples have been also included in Fig. 8.

After a strain of ε~3 (3 passes) the boundary distribution is inhomogeneous, being the shear bands aligned with the die shear plane (Fig. 8a). Many low misorientation and few high misorientation boundaries are observed. High misorientation gradients are introduced resulting in dislocation boundaries with moderate misorientation angles crossing original grain interiors. The fraction of high-angle grain boundaries (f_{HAB}) after 3 passes was 37%.

After eight passes (Fig. 8b), individual bands structures were no longer distinguishable from each other. At higher strains (ε~8), the grain boundary spacing was

further compressed and eventually a more uniform, finer, and highly elongated lamellar grain structure developed. The grains were aligned apparently with the shear direction of the last pass. These lamellar boundaries were predominantly high-angle in character but with few transverse HAGBs, and thus, f_{HAB} increased up to 56% after 8 passes.

The textures for the ECAP processed Al 7075-O samples at 130 ºC and different number of passes are given as pole figures in Fig. 8. These are typical FCC shear textures. FCC metals like aluminum, with high stacking fault energy, present stable shear textures consisting of a strong {hkl}<110> B fiber and a less strong {111}<uvw> A fiber [54], i.e., there is a strong tendency for the slip direction to become aligned with the shear direction. In aluminum, the ideal {100}<110> (C orientation) and {112}<110> (B orientation) components are normally positions of high orientation density on the B fiber [55].

Textures obtained after the early stages of ECAP (Fig. 8a) typically exhibit a few prominent orientations rather than continuous distributions along shear texture orientation fibers [8,54,56]. The shear texture is stronger with the increase of N_p up to 8p (Fig. 8b), where multiples orientations through the A and B fibers can be observed. The scatter about the predominant orientations in the discrete pole figures of Fig. 8 also suggests the presence of certain population of low-angle boundaries.

The (sub)grain microstructures for the Al 7075-O samples processed by 3 ECAP passes as a function of the processing temperature (80, 130 and 180 ºC) are shown in Fig. 9. The grains are elongated in the shear direction. The (sub)grain size in the perpendicular direction to the shear direction (L_Y) (Table 4) is reduced from L_Y >400 nm in the Al 7075-O processed by 1 ECAP pass (Fig. 7a) to 153 nm in the Al 7075-O alloy processed by 3p at 80 ºC (Fig. 9a). This processing path is the most severe considered in this study (highest processing stress), together with 8 passes at 130 ºC. Both paths result in similar (sub)grain sizes. The microstructure achieved after 3p-80 ºC (Fig. 9a) is characterized by high dislocation density within cells and (sub)grains. Fig. 9b and 9c show some microstructure changes when the ECAP processing is performed at higher temperature. The dislocation density within the cells obviously diminished as compared to those formed at lower temperature, and more defined cell boundaries were formed. The mean (sub)grain size increases with increasing processing temperature, being L_Y~318 nm at 180 ºC (Fig. 9c).

Microhardness measurements, summarized in Table 5, were carried out on the as-started material, and on the flow plane as a function of different ECAP processing conditions, number of passes and temperature. The as-started Al 7075-O shows a low microhardness value of 76 HV due to the coarsening of the hardening precipitates during the previous thermal treatment.

Severe deformation of the Al 7075-O samples results in a microhardness increase from 76 to 115 HV during the first ECAP pass. Then, the hardness increase occurs at a much lower rate with successive passes, reaching values of 133 HV at 130 ºC as the number of passes increases up to 8p. The high initial increase is attributed to the build up of high dislocation density that initiates (sub)grain walls [57].

The maximum microhardness of 135 HV has been achieved for the Al 7075-O ECAPed at the lowest processing temperature of 80 ºC and 3 passes (Table 5). Thus, the severe plastic straining produced at low temperature increases the strength of the Al 7075-O alloy by a factor of ~2, because the finest grain size (153 nm) and higher dislocation density is achieved after this processing condition. On the other hand, a processing temperature of 180 ºC causes a decrease in microhardness to 89 HV, due to the occurrence of grain growth (318 nm), and a rearrangement of the non-equilibrium grain boundaries into a lower energy structure (Fig. 9c).

4. Discussion

In the present work, the microstructure of an overaged Al 7075-O alloy processed by equal channel angular pressing (ECAP) has been characterized by TEM, and by an automated crystallographic orientation mapping (ACOM) tool attached to the transmission microscope. In addition, the maximum stress registered during ECAP processing has been considered as a good estimator of the stress applied on the sample during processing (σ_{Proc}). It is our contention, that this stress is a measure of the complex process history of the sample that determines the final grain size and it has been called "processing severity". Thus, the influence of the ECAP processing parameters determining the severity, such as the number of passes and temperature, on the microstructure has been considered. Microhardness measurements have been also performed in order to evaluate the mechanical properties at room temperature after ECAP processing.

4.1. Processing severity and microstructure

The processing severity (σ_{Proc}) has been properly characterized by the maximum stress reached during one ECAP pass (Fig. 2). Furthermore in Fig. 3, it has been shown that the first pass at room temperature is more severe (higher stress registered) than the next pass at 130 ºC and much more than at 180 ºC, due to higher recovery taking place at higher temperature. In fact, this figure is a clear demonstration that similar deformation degree, for example ε=3 after three passes at different temperatures, produces different grain sizes (Table 4), as a consequence of different processing stress on the sample. Even more interesting, according to the new concept introduced of

"processing severity", is the fact that samples having different deformations, for example ε=3 at 80 ºC or ε=8 at 130 ºC, have similar grain size of ~150 nm, and similar processing stress, as shown also in Fig.3, suggesting analogous severity levels reached during processing, which determine the (sub)grain sizes obtained.

On the other hand, the continuous stress increase after successive ECAP passes as shown in Fig.3 indicates that no discontinuous recrystallization processes have taken place, which would have led to material softening and thus lower resistance of the material to pass through the ECAP channel.

To emphasize the influence of the processing severity on the microstructure, Fig. 10 shows the relationship between σ_{Proc} and the (sub)grain size (L_Y), as a function of N_p and T_p. Therefore, this figure contains 5 different ECAP processing conditions and shows the inverse relations between the processing severity (σ_{Proc}) and the (sub)grain size. It seems from the exponential form of the curve that a value of L_Y close to saturation has been reached after 8 ECAP passes at 130 ºC or 3p at 80ºC. This saturation level is clearly observed in Fig. 3, where the degree of severity determined by σ_{Proc} increases with N_p up to 6-8 passes. Additionally, the processing temperatures considered in the present work, 80, 130 and 180 ºC, correspond to 0.38, 0.43 and 0.48 T_f respectively, and from a point of view of severe plastic deformation, they are considered intermediate temperatures, being above the normally accepted limit for cold deformation, which is $0.3T_f$. Higher T_p (180 ºC) decreases the processing severity because dynamic recovery processes by annihilation and rearrangement of dislocation are favored. Accordingly, if the pass severity (σ_{Proc}) decreases, the final (sub)grain size is bigger than that at low temperatures (Table 4).

On the other hand, for all processing conditions considered, the (sub)grain microstructures are usually elongated and aligned with the shear direction of the last pass (Figs. 7 and 9). The grain refining mechanism during ECAP-route B_C, which also leads to an increase in f_{HAB}, involves dynamic recovery (DRV) with continuous development of deformation bands (DBs), in general agreement with previous results [58]. Moreover, due to the 90º rotation in the same sense between consecutive passes (route B_C), new bands intersected the previously formed bands [59]. At these intersections relatively large misorientations developed, hence leading to the formation of new HAGBs. The highest strain after 8 ECAP passes (ε~8) leads to the gradual build-up of higher misorientation between the neighboring subgrains, increasing f_{HAB} up to 56% (Fig. 8b).

From the presented results, it is concluded that the "processing severity" or processing stress determines the grain size, and the total strain determines the obtained misorientation degree.

4.2. Comparison with pure aluminum

The final (sub)grain sizes obtained for ECAPed Al 7075-O are smaller than those obtained for pure aluminum (~1.1 μm) processed by 8 passes of ECAP by B_C route at room temperature with an equivalent strain of ε~8 [60]. In the present study, the as-started material was overaged to avoid precipitate nucleation from the solid solution and/or coarsening during ECAP processing. The Al 7075-O alloy has coarse precipitates, mainly Mg(Zn_2,AlCu) and $Al_{18}Mg_3Cr_2$ that are 100 to 200 nm in size, and the solid solution has been removed during the heat treatment. Therefore, the main difference with pure aluminum is the presence of these second phase particles, which are responsible of the higher refining for the ECAPed Al 7075-O respect to pure aluminum.

Re-dissolution and possible re-precipitation of precipitates during ECAP processing at room temperature has been reported for initial microstructures containing very fine precipitates, and at high stress levels due to the low processing temperature [61-63]. However, at the temperatures and ECAP conditions considered in this study, no re-dissolution, or re-precipitation or even cracking of particles take place, as it has been shown in the TEM micrographs of Fig. 6 and 7. The occurrence of precipitate fragmentation during ECAP was reported earlier for θ′ precipitates in an Al–Cu alloy [61], β′ precipitates in an Al–Mg–Si alloy [64] and $MgZn_2$ precipitates in an Al-7050 alloy [27] with elongated morphologies. However, in the present overaged alloy, the spherical morphology makes more difficult the fracture of precipitates during processing [65]. Furthermore, it is expected that they remain constant during additional processes, such as superplastic forming or other thermal treatments, inhibiting simultaneous processes of recovery and recrystallization.

It has been reported that the presence of second phase particles affects the generation and rearrangement of dislocations during severe plastic deformation [66-68]. “Geometrically necessary dislocations” are generated in the aluminum matrix surrounding the second phase particles to accommodate the plastic deformation, together with the statistically stored dislocations in an aluminum matrix without second phase particles [69-71]. This high density of dislocations, distributed between the precipitates is a strong driving force for more rapid substructure generation, and for continued structural refinement with increased strain.

On the other hand, the fraction of high-angle grain boundaries (f_{HAB}) increases with N_p. f_{HAB} increases from ~37% after 3 ECAP passes to ~56% after 8 passes, according to the values obtained by ACOM-TEM. These values have been compared with those obtained for pure aluminum (Fig. 11) subjected to similar ECAP processing, reaching a

f_{HAB} value of about 70% [8]. These data clearly show an increase in the population of high-angle boundaries associated with repetitive ECAP operations for both materials. However, the most important increase in the population of high-angle boundaries is produced during the first four passes due to development of fine grains along original grain boundaries, and large-scale DBs crossing the grain interiors [72]. Beyond four passes, f_{HAB} proceeds to grow with increasing strain, and finally approach saturation values of about 0.6 for the Al 7075-O alloy and 0.8 for pure aluminum at N_p~12. The lower fraction of HABs for the Al 7075-O alloy than for the pure aluminum at high strains is due to the fact that during plastic deformation the second phase particles present a barrier to dislocation motion so that dislocation networks form around particles [67]. Accordingly, the fraction of LABs in the Al 7075-O alloy is relatively high even after 8 passes, equivalent to ε~8.0 in comparison with the pure aluminum. This is characteristic of a deformation induced microstructure [73-78], where the particles contribute to increase the dislocation density in the present alloy, and LABs are continuously formed during strain through successive ECAP passes.

4.3. Vickers microhardness

Finally, the hardness exhibited a marked increase from 76 HV in the as-started material to 133 HV in the material subjected to 8 ECAP passes at 130 ºC, and 135 HV after 3 ECAP passes at a lower processing temperature (Table 5). These microhardness values achieved after the most severe processing conditions are very similar, and they are mainly determined by the (sub)grain sizes obtained after both processing paths (Table 3 and 4). On the other hand, the hardness slowly increases with N_p, being 120 HV for three passes and 133 HV for eight passes. Previous results [60,79] showed that there is no significant change in the hardness distributions in pure Al after four ECAP passes. However, our results are in agreement with an earlier report on Al–Mg alloys [80], where an increase in the microhardness value was shown up to higher number of ECAP passes, due to the lower rates of recovery in the alloys [43,81]. This slow recovery leads to finer grain sizes in alloys after ECAP processing than in pure Al, being necessary to impose a larger number of passes in order to establish a highly misoriented microstructure [82].

In addition, the major strengthening factors for the processed samples respect to the as-started Al 7075-O sample will be on one side, as mentioned, the grain refinement strengthening by the Hall–Petch effect, and on the other side, the high density of dislocations retained inside the grains, especially after the first pass of deformation, as illustrated in Fig. 7a, or at the lowest processing temperature (Fig. 9a). It is considered that the contribution by Orowan hardening of the coarsened precipitates present in the

as-started alloy is small, because they remain relatively separated and furthermore they are mainly at grain boundaries.

Lastly, Table 5 shows a strong decrease of hardness with increasing processing temperature for three passes, 89 vs 135 HV. This is attributed to the effect of both an increase in grain size and dynamic recovery.

In summary, high strength Al 7075 alloy was subjected to severe plastic deformation by ECAP, starting from an overaged state and obtaining good surface quality with no visible cracking. An ultrafine grained microstructure with grain sizes of about 150 nm has been developed after the most severe processing conditions, which will be very helpful to achieve superplastic forming at high strain rates. Furthermore, from stress raw data we have provided a relationship between stress and final microstructure for a SPD processing, which possesses a higher prediction capability than the deformation concept.

5. Conclusions

In the present work, the microstructure of an overaged Al 7075-O alloy processed by ECAP-route B_C has been characterized as a function of number of passes and processing temperature. Both processing variables determine the processing severity. The major conclusions of the study are as follows:

1. The higher is the total strain (N_p) and the lower the processing temperature (T_p), i.e. the higher is the processing severity, the finer is the (sub)grain size obtained. The processing severity has been properly estimated by σ_{max} of an ECAP pass. The (sub)grain size decreases with strain at a given processing temperature, and a (sub)grain size value close to saturation seems to be reached after 8 ECAP passes at 130 ºC. Accordingly, the smallest grain size observed was about 150 nm for samples processed by 3p at 80 ºC or 8p at 130 ºC.
2. Severe plastic deformation at higher temperature (180 ºC) decreases the processing severity and leads to a coarser grain size and lower dislocation density by dynamic recovery processes. As a result, a lower microhardness value was obtained.
3. The grain size obtained for the ECAP processed Al 7075-O alloy is finer than for pure aluminum due to the presence of second phase particles in the overaged alloy such as $Mg(Zn_2,AlCu)$ and $Al_{18}Mg_3Cr_2$, with particle sizes about 100-200 nm. Dislocations generated during the severe plastic deformation are trapped by the second phase particles, modifying the evolution of the (sub)grain microstructure during ECAP processing.

4. An automated crystallographic orientation mapping (ACOM) tool attached to the transmission electron microscope allowed characterizing the texture and misorientation distribution of the severely deformed Al 7075-O alloy. The ECAP processed samples showed a simple shear texture. The strain increase enhances the presence of high-angle grain boundaries. The maximum f_{HAB} value was about 56% for Al 7075-O samples processed by 8 passes at 130 ºC, being this value lower than that for pure aluminum (f_{HAB}~70%) subjected to similar ECAP processing. This is because the particles in the present alloy contribute to increase the dislocation density, and LABs are continuously formed during strain through successive ECAP passes.

Acknowledgements

Financial support from MICINN (Project MAT2009-14452) is gratefully acknowledged.

References

1. J.E. Hatch (Ed.), Aluminium: Properties and Physical Metallurgy, American Society for Metals, Ohio, 1984, pp.370.
2. G. Fribourg, Y. Bréchet, J.L. Chemin and A. Deschamps: Metall. Mater. Trans. A, 2011, In press.
3. C.M. Cepeda-Jiménez, P. Hidalgo, M. Pozuelo, O.A. Ruano and F. Carreño: Mater. Sci. Eng. A, 2010, vol. 527, pp. 2579-2587.
4. A.P. Zhilyaev, D.L. Swisher, K. Oh-ishi, T.G. Langdon and T.R. McNelley: Mater. Sci. Eng. A, 2006, vol. 429, pp. 137-148.
5. R.Z. Valiev, N.A. Krasilnikov and N.K. Tsenev: Mater. Sci. Eng. A, 1991, vol. 137, pp. 35-40.
6. R.Z. Valiev, R.R. Mulyukov, V.V. Ovchinnikov and V.A. Shabashov: Scripta Metall. Mater., 1991, vol. 25, pp. 2717-2722.
7. N.A. Akhmadeev, N.P. Kobelev, R.R. Mulyukov, M.Ya. Soifer and R.Z. Valiev: Acta Metall. Mater., 1993, vol. 41, pp. 1041-1046.
8. S.D. Terhune, D.L. Swisher, K. Oh-Ishi, Z. Horita, T.G. Langdon and T.R. McNelley: Metall. Mater. Trans. A, 2002, vol. 33, pp. 2173-2184.
9. J.M. García-Infanta, S. Swaminathan, A.P. Zhilyaev, F. Carreño, O.A. Ruano and T.R. McNelley: Mater. Sci. Eng. A, 2008, vol. 485, pp. 160-175.
10. J.M. García-Infanta, S. Swaminathan, C.M. Cepeda-Jiménez, T.R. McNelley, O.A. Ruano and F. Carreño: J. Alloys Compd., 2009, vol. 478, pp. 139-143.
11. L. Balogh, R.B. Figueiredo, T. Ungár and T.G. Langdon: Mater. Sci. Eng. A, 2010, vol. 528, pp. 533-538.
12. V.M. Segal: Mater. Sci. Eng. A, 1995, vol. 197, pp. 157-164.
13. T.G. Langdon: Rev. Metal. Madrid, 2008, vol. 44, pp. 556-564.
14. K. Oh-Ishi, Z. Horita, M. Furukawa, M. Nemoto and T.G. Langdon: Metall. Mater. Trans. A, 1998, vol. 29, pp. 2011-2013.
15. Y. Iwahashi, J. Wang, Z. Horita, M. Nemoto and T.G. Langdon: Scripta Mater., 1996, vol. 35, pp. 143-146.
16. Y. Iwahashi, Z. Horita, M. Nemoto and T.G. Langdon: Acta Mater., 1998, vol. 46, pp. 3317-3331.
17. H. Kim, M. Soe and S. Hong: Mater. Sci. Eng. A, 2000, vol. 291, pp. 86-90.
18. T. Aida, K. Matsuki, Z. Horita and T.G. Langdon: Scripta Mater., 2001, vol. 44, pp. 575-579.
19. J. Suh, H. Kim, J. Park and J. Chang: Scripta Mater., 2001, vol. 44, pp. 677-681.
20. S.J. Oh and S.B. Kang: Mater. Sci. Eng. A, 2003, vol. 343, pp. 107-115.

21. C. Xu and T.G. Langdon: Scripta Mater., 2003, vol. 48, pp. 1-4.
22. D. Shin, D. Hwang, Y. Oh and K. Park: Metall. Mater. Trans. A, 2004, vol. 35, pp. 825-837.
23. K. Turba, P. Málek, E.F. Rauch and M. Cieslar: Mater. Sci. Forum, 2008, vol. 584-586, pp. 164-169.
24. K. Turba, P. Málek, E.F. Rauch, F. Robaut and M. Cieslar: Int. J. Mater. Res., 2009, vol. 100, pp. 851-857.
25. Z.L. Ning, S. Guo, F.Y. Cao, G.J. Wang, Z.C. Li and J.F. Sun: J. Mater. Sci., 2010, vol. 45, pp. 3023-3029.
26. L.J. Zheng, C.Q. Chen, T.T. Zhou, P.Y. Liu and M.G. Zeng: Mater. Charact., 2002, vol. 49, pp. 455-461.
27. C.Y. Nam, J.H. Han, Y.H. Chung and M.C. Shin: Mater. Sci. Eng. A, 2003, vol. 347, pp. 253-257.
28. Y.H. Zhao, X.Z. Liao, R.Z. Valiev and Y.T. Zhu: Acta Mater., 2004, vol. 52, pp. 4589-4599.
29. P. Málek, M. Cieslar and R.K. Islamgaliev: J. Alloys Compd., 2004, vol. 378, pp. 237-241.
30. Y.H. Zhao, X.Z. Liao, R.Z. Valiev and Y.T. Zhu: J. Mater. Research, 2005, vol. 20, pp. 288-291.
31. G. Sha, Y.B. Wang, X.Z. Liao, Z.C. Duan, S.P. Ringer and T.G. Langdon: Acta Mater., 2009, vol. 57, pp. 3123-3132.
32. Z.C. Duan, N.Q. Chinh, C. Xu and T.G. Langdon: Metall. Mater. Trans. A, 2010, vol. 41, pp. 802-809.
33. S. Lee, A. Utsunomiya, H. Akamatsu, K. Neishi, M. Furukawa, Z. Horita and T.G. Langdon: Acta Mater., 2003, vol. 50, pp. 553-564.
34. C. Xu, M. Furukawa, Z. Horita and T.G. Langdon: Acta Mater., 2003, vol. 51, pp. 6139-6149.
35. A. Momeni and K. Dehghani: Metall. Mater. Trans. A, 2011, vol. 42, pp. 1925-1932.
36. M.Carsí, V. López, F. Peñalba and O.A. Ruano: Mater. Sci. Eng. A, 1996, vol. 216, pp. 155-160.
37. M. Eddahbi, J.A. Jiménez and O.A. Ruano: J. Alloys Compd., 2007, vol. 433, pp. 97-107.
38. J.A. Jiménez, M. Carsí, G. Frommeyer, S. Knippscher, J. Witting and O.A. Ruano: Intermetallics, 2005, vol. 13, pp. 1021-1029.
39. P.J. Apps, M. Berta and P.B. Prangnell: Acta Mater., 2005, vol. 53, pp. 499-511.

40. P. Kumar, C. Xu and T.G. Langdon: Mater. Sci. Eng. A, 2006, vol. 429, pp. 324-328.
41. N. Kamikawa, X. Huang, N. Tsuji and N. Hansen: Acta Mater., 2009, vol. 57, pp. 4198-4208.
42. M.T. Pérez-Prado, J.A. del Valle and O.A. Ruano: Scripta Mater., 2004, vol. 51, pp. 1093-1097.
43. A.P. Zhilyaev and T.G. Langdon: Progress Mater. Sci., 2008, vol. 53, pp. 893-979.
44. R.Z. Valiev and T.G. Langdon: Progress Mater. Sci., 2006, vol. 51, pp. 881-981.
45. O.D. Sherby and P.M. Burke: Progress Mater. Sci., 1968, vol. 13, pp. 323-390.
46. S. Komura, M. Furukawa, Z. Horita, M. Nemoto and T.G. Langdon: Mater. Sci. Eng. A, 2001, vol. 297, pp. 111-118.
47. G. Shigesato and E.F. Rauch: Mater. Sci. Eng. A, 2007, vol. 462, pp. 402-406.
48. E.F. Rauch and M. Veron: Materialwissenschaft und Werkstofftechnick, 2005, vol. 36, pp. 552-556.
49. E.R Rauch and A. Duft: Mater. Sci. Forum, 2005, vol. 495- 497, pp. 197-202.
50. F.J. Humphreys and M. Hatherly: Recrystallization and Related Annealing Phenomenon, 2nd ed., Elsevier, Oxford, UK, 2004, pp.70-71.
51. J.A. Wert: Scripta Metall., 1981, vol. 15, pp. 445-447.
52. R.Ayer, J.Y. Koo, J.W. Steeds and B.K. Park: Metall. Trans. A, 1985, vol. 16, pp. 1925-1936.
53. R.Z. Valiev, R.K. Islamgaliev, N.F. Kuzmina, Y. Li and T.G. Langdon: Scripta Mater., 1999, vol. 40, pp. 117-122.
54. A. Gholinia, P. Bate and P.B. Prangnell: Acta Mater., 2002, vol. 50, pp. 2121-2136.
55. G.R. Canova, U.F. Kocks and J.J. Jonas: Acta Metall., 1984, vol. 32, pp. 211-226.
56. L.S. Tóth, R.A. Massion, L. Germain, S.C. Baik and S. Suwas: Acta Mater., 2004, vol. 52, pp. 1885-1898.
57. E.A. El-Danaf: Mater. Sci. Eng. A, 2007, vol. 487, pp. 189-200.
58. T.R. McNelley, D.L. Swisher, in: Y.T. Zhu, T.G. Langdon, R.Z. Valiev, S.L. Semiatin, D.H. Shin and T.C. Lowe (Eds.): TMS Symposium Ultrafine Grained Materials, 2004, vol. 3, pp. 89-94.
59. J. C. Werenskiold and H. J. Roven: Mater. Sci. Eng. A, 2005, vol. 410-411, pp. 174-177.
60. C. Xu, M. Furukawa, Z. Horita and T.G. Langdon: Mater. Sci. Eng. A, 2005, vol. 398, pp. 66-76.
61. M. Murayama, Z. Horita and K. Hono: Acta Mater., 2001, vol. 49, pp. 21-29.

62. I. Gutierrez-Urrutia, M.A. Muñoz-Morris and D.G. Morris: Mater. Sci. Eng. A, 2005, vol. 394, pp. 399-410.
63. Z.Liu, S. Bai, X. Zhou and Y. Gu: Mater. Sci. Eng. A, 2011, vol. 528, pp. 2217-2222.
64. K. Oh-Ishi, Y. Hashi, A. Sadakata, K. Kaneko, Z. Horita and T.G. Langdon: Mater. Sci. Forum, 2002, vol. 396-402, pp. 333-338.
65. G. Guiglionda and W.J. Poole: Mater. Sci. Eng. A, 2001, vol. 319-321, pp. 583-587.
66. A. Goloborodko, O. Sitdikov, R. Kaibyshev, H. Miura and T. Sakai: Mater. Sci. Eng. A, 2004, vol. 381, pp. 121-128.
67. H. Cao, J.Y. Min, S.D. Wu, A.P. Xian and J.K. Shang: Mater. Sci. Eng. A, 2006, vol. 431, pp. 86-91.
68. H.J. Roven, M. Liu and J.C. Werenskiold: Mater. Sci. Eng. A, 2008, vol. 483-484, pp. 54-58.
69. P.B. Trivedi, R.S. Yassar, D.P. Field and R. Alldredge: Mater. Sci. Eng. A, 2006, vol. 425, pp. 205-212.
70. M.A. Muñoz-Morris, I. Gutierrez-Urrutia and D.G. Morris: Mater. Sci. Eng. A, 2008, vol. 493, pp. 141-147.
71. J. Zhang, N. Gao and M.J. Starink: Mater. Sci. Eng. A, 2010, vol. 527, pp. 3472-3479.
72. O. Sitdikov, T. Sakai, H. Miura and C. Hama: Mater. Sci. Eng. A, 2009, vol. 516, pp. 180-188.
73. C.Y.Yu, P.L. Sun, P.W. Kao and C.P. Chang: Mater. Sci. Eng. A, 2004, vol. 366, pp. 310-317.
74. O. Sitdikov, T. Sakai, A. Goloborodko, H. Miura and R. Kaibyshev: Philos. Mag., 2005, vol. 85, pp. 1159-1175.
75. C. Kobayashi, T. Sakai, A. Belyakov and H. Miura: Philos. Mag. Lett., 2007, vol. 87, pp. 751-766.
76. I. Mazurina, T. Sakai, H. Miura, O. Sitdikov and R. Kaibyshev: Mater. Sci. Eng. A, 2008, vol. 473, pp. 297-305.
77. T. Sakai, A. Belyakov and H. Miura: Metall. Mater. Trans. A, 2008, vol. 39, pp. 2206-2214.
78. I.Mazurina, T. Sakai, H.Miura, O. Sitdikov and R. Kaibyshev: Mater. Trans., 2009, vol. 50, pp. 101–110.
79. S.N. Alhajeri, N. Gao and T.G. Langdon: Mater. Sci. Eng. A, 2011, vol. 528, pp. 3833-3840.

80. Y. Iwahashi, Z. Horita, M. Nemoto and T.G. Langdon: Metall. Mater. Trans. A, 1998, vol. 29, pp. 2503-2510.
81. R. Roumina and C.W. Sinclair: Acta Mater., 2010, vol. 58, pp. 111-121.
82. C. Xu, Z. Horita and T.G. Langdon: Mater. Sci. Eng. A, 2011, vol. 528, pp. 6059-6065.

Figure Captions

Fig. 1. Scheme of the ECAP processing of Al 7075-O samples by route B_C.

Fig. 2. Load-displacement curve obtained during the first ECAP pass.

Fig. 3. Evolution of processing stress vs number of passes at different temperatures, as a measure of processing severity.

Fig. 4. Isometric optical micrographs showing the microstructure of the as-started Al 7075-O alloy.

Fig. 5. EBSD map and corresponding pole figures of the ND-RD section of the as-started Al 7075-O alloy.

Fig. 6. TEM micrograph and EDX spectra corresponding to precipitates present in the as-started Al 7075-O alloy.

Fig. 7. TEM micrographs showing the microstructure of the Al 7075-O after ECAP processing as a function of the number of passes: a) 1p-T_{RT}; b) 3p-130 ºC; c) 5p-130 ºC and d) 8p-130 ºC. The insets show the corresponding SAED patterns, and the black arrows show the location of some precipitates.

Fig. 8. Orientation maps and pole figures obtained by an automated electron diffraction pattern indexing tool attached to the TEM (ACOM-TEM) of the Al 7075-O alloy after ECAP processing: a) 3p-130 ºC; b) 8p-130 ºC.

Fig. 9. TEM micrographs showing the microstructure of the Al 7075-O after ECAP processing as a function of the temperature: a) 3p-80 ºC; b) 3p-130 ºC and c) 3p-180 ºC.

Fig. 10. σ_{Proc} versus L_Y for the Al 7075-O alloy after ECAP processing as a function of the number of passes and processing temperature.

Fig. 11. Fraction of high-angle boundaries (f_{HAB}) for pure aluminium [7] and Al 7075-O alloy after ECAP processing by route B_C as a function of the number of passes.

Table 1. Chemical composition of the as-received Al 7075 alloy (wt%).

Si	Fe	Zn	Mg	Cu	Cr	Mn	Ti	Al
0.052	0.19	5.68	2.51	1.59	0.19	0.007	0.025	balance

Table 2. Nomenclature used for the as-started Al 7075 alloy and ECAP processed samples.

Processing	Nomenclature
Al 7075-T651 + overaging during 5h at 280 ºC	Al 7075-O
1 pass at room temperature (T_{RT})	1p T_{RT}
1 pass at T_{RT} + 2 passes at 130 ºC	3p 130 ºC
1 pass at T_{RT} + 4 passes at 130 ºC	5p 130 ºC
1 pass at T_{RT} + 7 passes at 130 ºC	8p 130 ºC
1 pass at T_{RT} + 2 passes at 80 ºC	3p 80 ºC
1 pass at T_{RT} + 2 passes at 180 ºC	3p 180 ºC

Table 3. (Sub)grain size (L_Y) measurements of the Al 7075-O alloy after ECAP processing at 130 ºC as a function of the number of passes.

Processing	**L_Y (nm)**
1p T_{RT}	> 400
3p 130 ºC	200 ± 5
5p 130 ºC	175 ± 6
8p 130 ºC	163 ± 5

Table 4. (Sub)grain size (L_Y) measurements of the Al 7075-O alloy after 3 passes of ECAP processing at different temperatures.

Processing	**L_Y (nm)**
3p 80 ºC	153 ± 5
3p 130 ºC	200 ± 6
3p 180 ºC	318 ± 17

Table 5. Microhardness Vickers (0.5 kg; 15 s) values of the as-started Al 7075-O alloy and after ECAP processing.

Processing	**HV**
Al 7075-O	76 ± 1
1p T_{RT}	115 ± 1
3p 130 ºC	120 ± 2
5p 130 ºC	130 ± 1
8p 130 ºC	133 ± 1
3p 80 ºC	135 ± 3
3p 180 ºC	89 ± 1

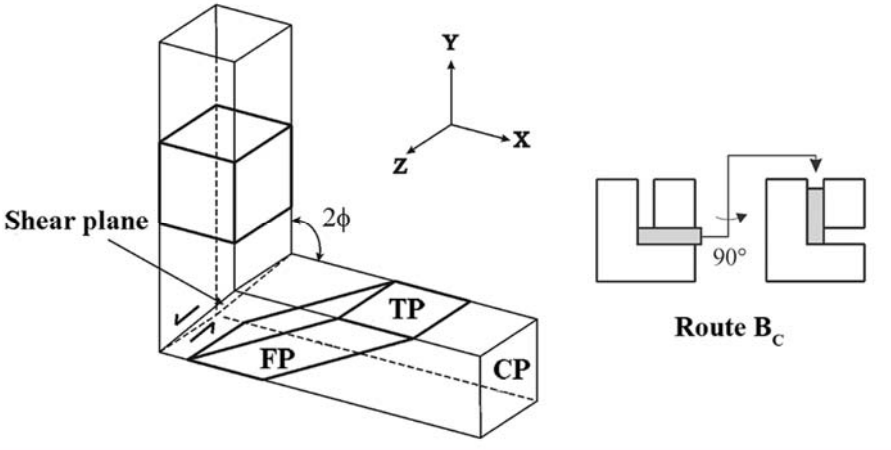

Fig. 1. Scheme of the ECAP processing of Al 7075-O samples by route B_C.

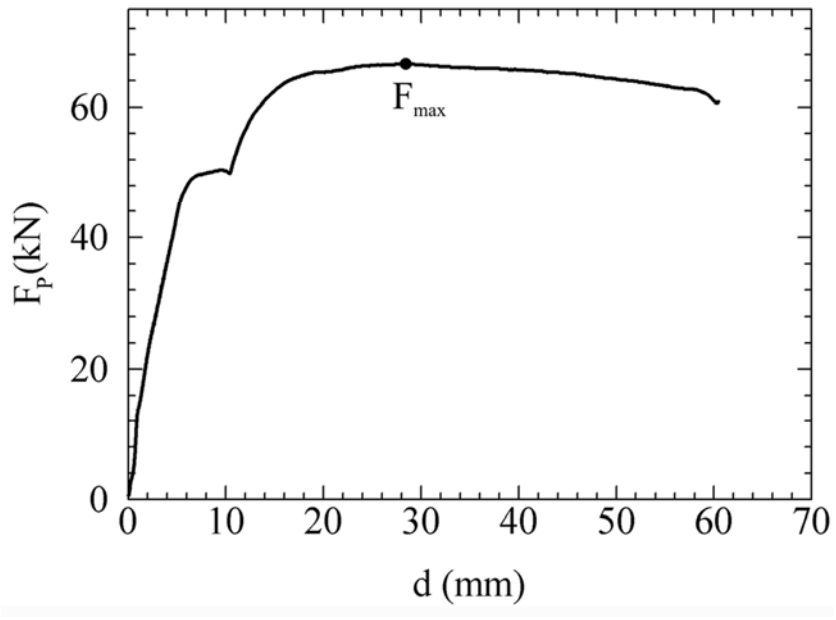

Fig. 2. Load-displacement curve obtained during the first ECAP pass.

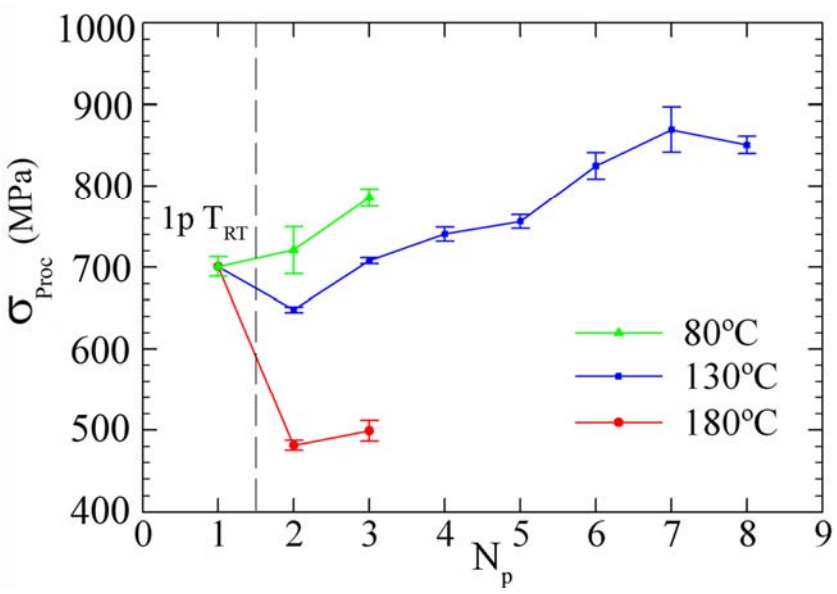

Fig. 3. Evolution of processing stress vs number of passes at different temperatures, as a measure of processing severity.

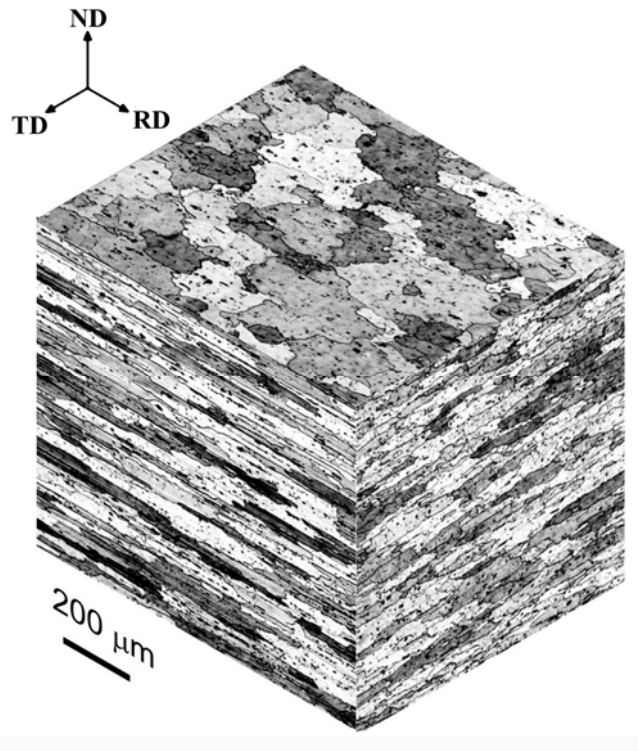

Fig. 4. Isometric optical micrographs showing the microstructure of the as-started Al 7075-O alloy.

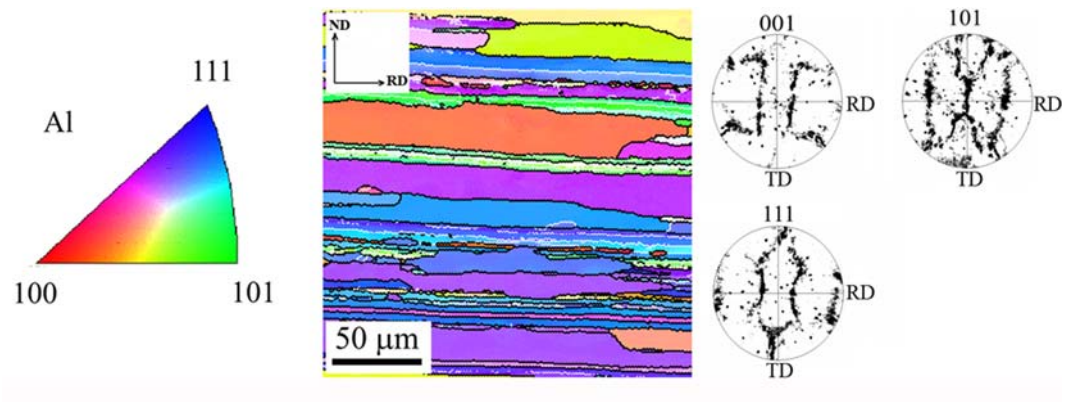

Fig. 5. EBSD map and corresponding pole figures of the ND-RD section of the as-started Al 7075-O alloy.

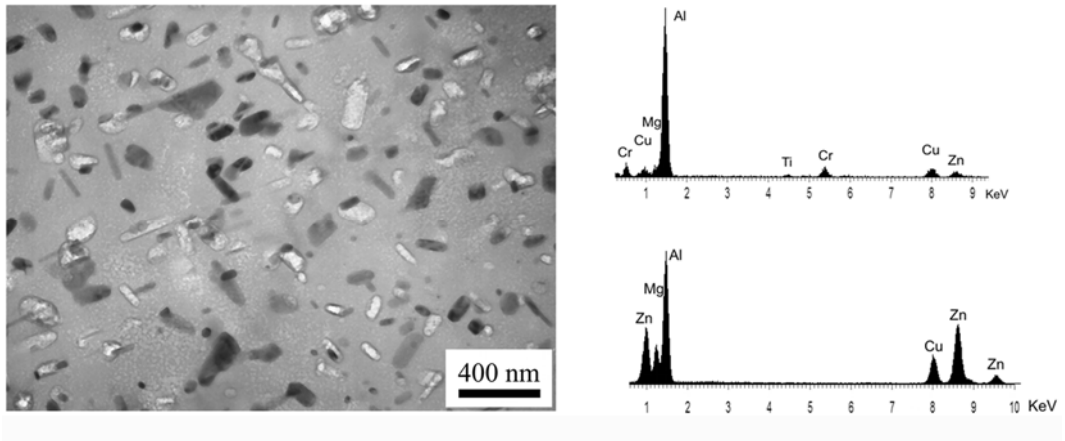

Fig. 6. TEM micrograph and EDX spectra corresponding to precipitates present in the as-started Al 7075-O alloy.

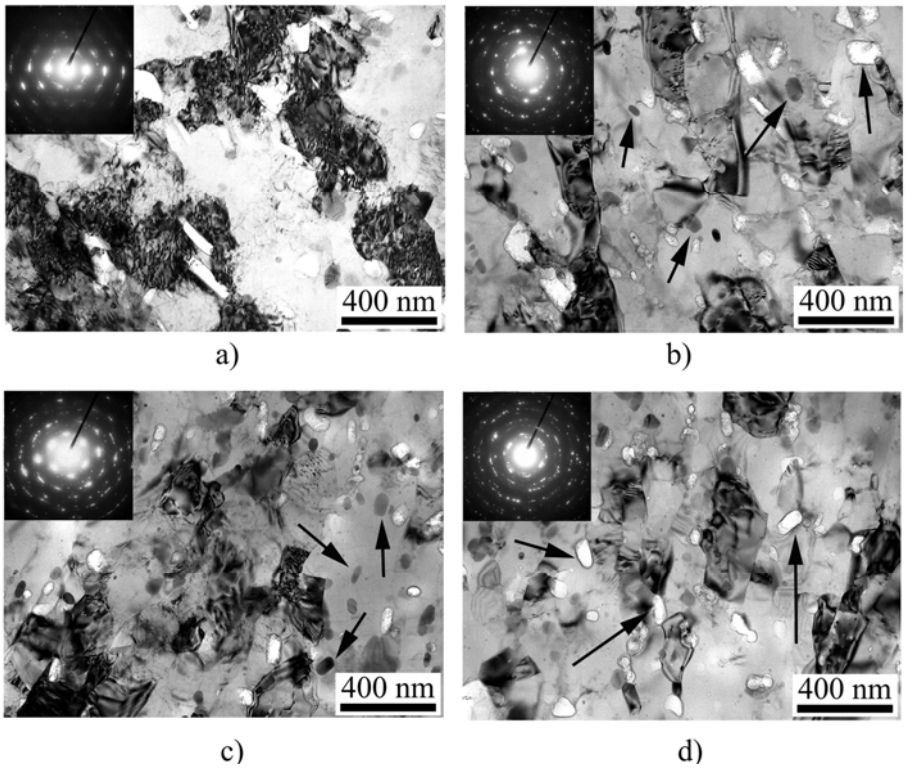

Fig. 7. TEM micrographs showing the microstructure of the Al 7075-O after ECAP processing as a function of the number of passes: a) 1p-T_{RT}; b) 3p-130 ºC; c) 5p-130 ºC and d) 8p-130 ºC. The insets show the corresponding SAED patterns, and the black arrows show the location of some precipitates.

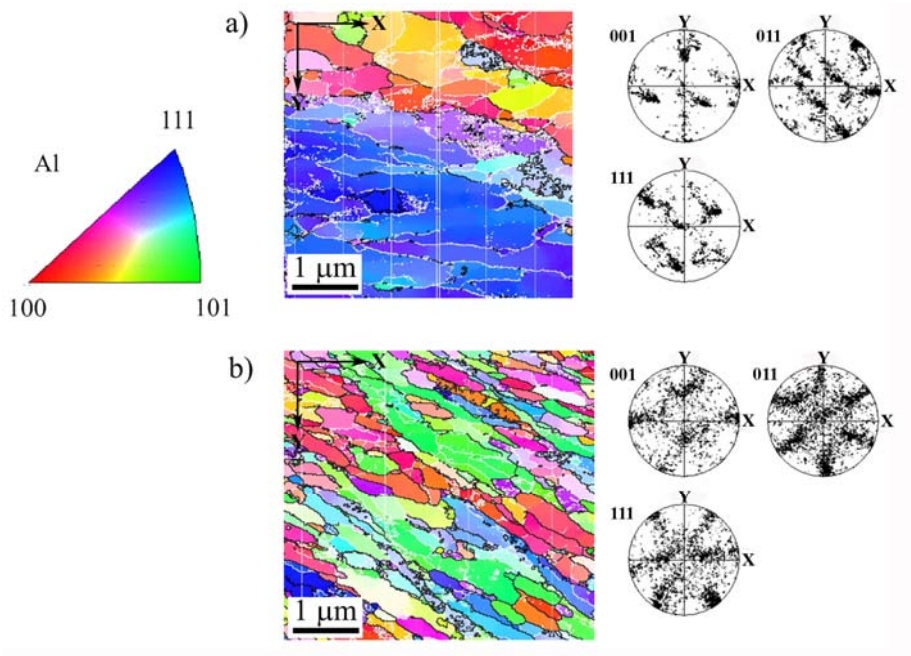

Fig. 8. Orientation maps and pole figures obtained by an automated electron diffraction pattern indexing tool attached to the TEM (ACOM-TEM) of the Al 7075-O alloy after ECAP processing: a) 3p-130 ºC; b) 8p-130 ºC.

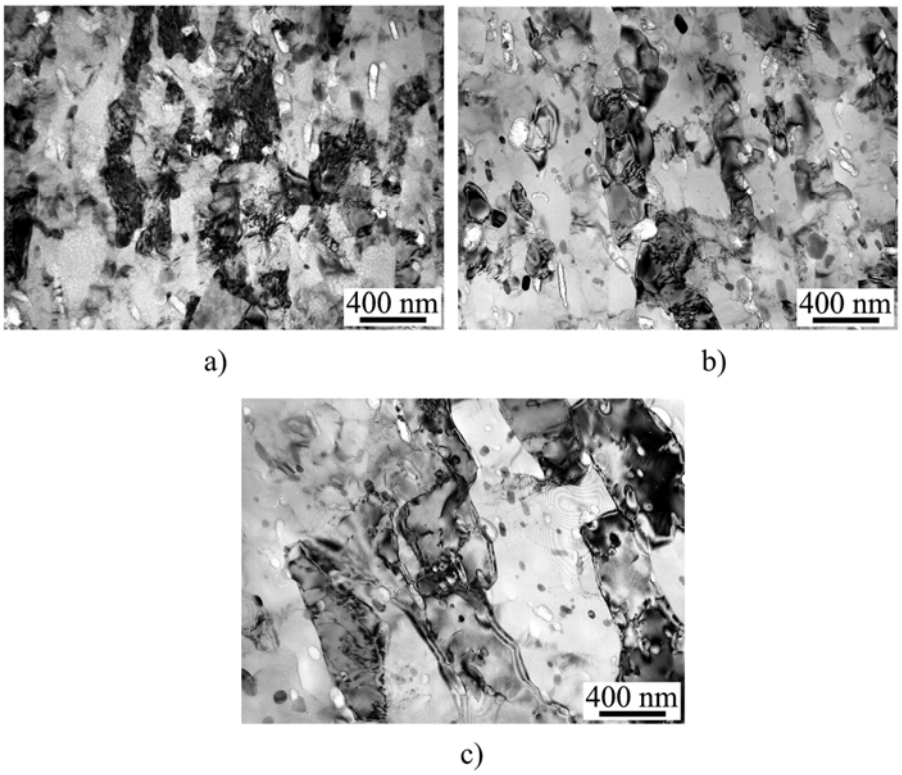

Fig. 9. TEM micrographs showing the microstructure of the Al 7075-O after ECAP processing as a function of the temperature: a) 3p-80 ºC; b) 3p-130 ºC and c) 3p-180 ºC.

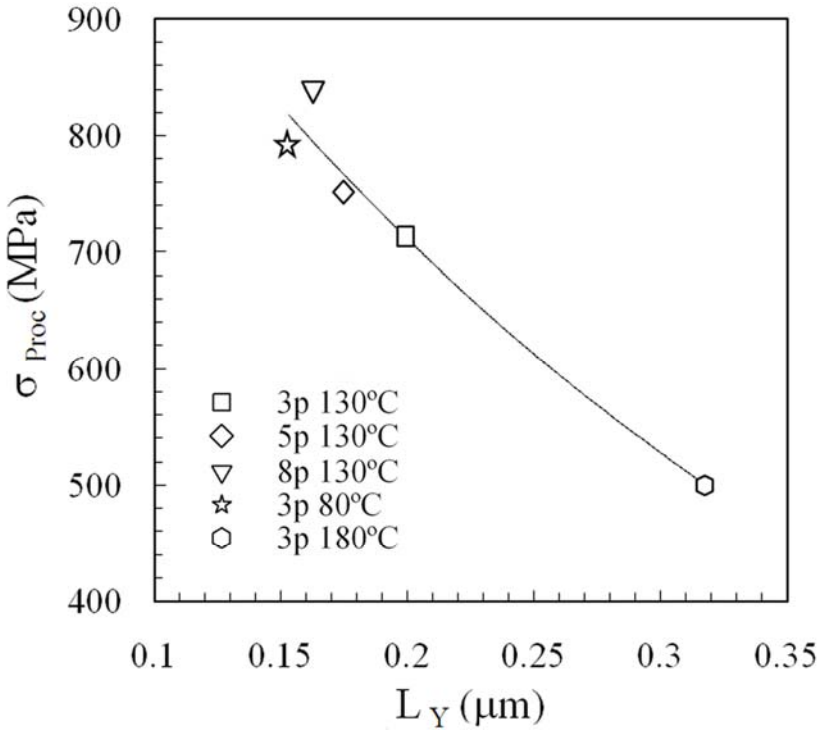

Fig. 10. σ_{Proc} versus L_Y for the Al 7075-O alloy after ECAP processing as a function of the number of passes and processing temperature.

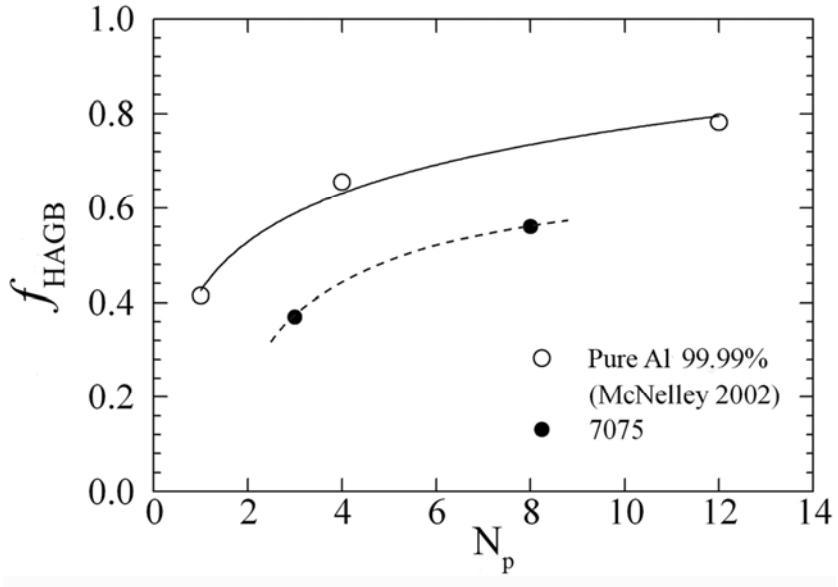

Fig. 11. Fraction of high-angle boundaries (f_{HAB}) for pure aluminium [7] and Al 7075-O alloy after ECAP processing by route B_C as a function of the number of passes.